Nano-topography and functionalization with the synthetic peptoid GN2-Npm9 as a strategy for antibacterial and biocompatible titanium implants

(Article begins on next page)

11 February 2024

Research article

Nano-topography and functionalization with the synthetic peptoid GN2-Npm$_9$ as a strategy for antibacterial and biocompatible titanium implants

Francesca Gamna [a],[*], Andrea Cochis [c], Biljana Mojsoska [b], Ajay Kumar [c], Lia Rimondini [c], Silvia Spriano [a]

[a] *Politecnico di Torino, Turin, Italy*
[b] *Department of Science and Environment, Roskilde University, Roskilde, Denmark*
[c] *Università del Piemonte Orientale UPO, Department of Health Sciences, Center for Translational Research on Autoimmune and Allergic Diseases–CAAD, Novara, Italy*

A B S T R A C T

In recent years, antimicrobial peptides (AMPs) have attracted great interest in scientific research, especially for biomedical applications such as drug delivery and orthopedic applications. Since they are readily degradable in the physiological environment, scientific research has recently been trying to make AMPs more stable. Peptoids are synthetic N-substituted glycine oligomers that mimic the structure of peptides. They have a structure that does not allow proteolytic degradation, which makes them more stable while maintaining microbial activity. This structure also brings many advantages to the molecule, such as greater diversity and specificity, making it more suitable for biological applications. For the first time, a synthesized peptoid (GN2-Npm$_9$) was used to functionalize a nanometric chemically pre-treated (CT) titanium surface for bone-contact implant applications. A preliminary characterization of the functionalized surfaces was performed using the contact angle measurements and zeta potential titration curves. These preliminary analyses confirmed the presence of the peptoid and its adsorption on CT. The functionalized surface had a hydrophilic behaviour (contact angle = 30°) but the hydrophobic tryptophan-like residues were also exposed. An electrostatic interaction between the lysine residue of GN2-Npm$_9$ and the surface allowed a chemisorption mechanism. The biological characterization of the CT_GN2-Nmp$_9$ surfaces demonstrated the ability to prevent surface colonization and biofilm formation by the pathogens *Escherichia coli* and *Staphylococcus epidermidis* thus showing a broad-range activity. The cytocompatibility was confirmed by human mesenchymal stem cells. Finally, a bacteria-cells co-culture model was applied to demonstrate the selective bioactivity of the CT_GN2-Nmp$_9$ surface that was able to preserve colonizing cells adhered to the device surface from bacterial infection.

1. Introduction

Antimicrobial peptides (AMPs) have become increasingly important in biomedical applications due to their different and multiple

---

abilities. However, AMPs are not without limitations, particularly concerning their stability. One of the major limitations of peptides in biomedical applications is proteolytic degradation. Peptides can be rapidly degraded by proteases in the body, which can result in a short half-life and reduced bioavailability [1]. Other limitations regard chemical reactions, such as oxidation, hydrolysis, and race-mization which can affect the AMPs' stability and functionality [2,3]. Moreover, they often have greater problems of solubility in water or biological fluids, which can limit their bioavailability and efficacy [4]. Additionally, peptides can be sensitive to temperature changes, which can affect their stability and functionality [5]. Another limitation of peptides in biomedical applications is their potential for immunogenicity. They can be recognized as foreign bodies by the immune system, leading to an immune response that can limit their effectiveness and cause adverse reactions [2].

To overcome these limitations, efforts are being made to develop new strategies focused on the improvement of peptides' stability. For these reasons, peptoids have been introduced as an alternative to peptides. Peptides and peptoids are two classes of molecules that are similar in structure but differ in several key features. Peptides are short chains of amino acids that are linked together by peptide bonds. Peptoids, on the other hand, are synthetic molecules that resemble peptides but have their side chains (R) attached to the nitrogen atoms instead of the alpha-carbon atoms. This difference in structure gives peptoids several advantages over peptides, including increased stability, diversity, and specificity. Peptoids are more stable than peptides because the side chains are not sus-ceptible to cleavage by protease or acid hydrolysis, they are more bioavailable and have more stability to ionic strength and pH variations [6]. These properties make peptoids more suitable for use in biological applications that require long-term stability, such as drug development. Moreover, peptoids are highly flexible in composition and can be synthesized with a wide range of side chains. This diversity allows for the creation of large libraries of peptoids that can be screened for specific biological activities. Peptoids have a high degree of specificity due to their unique structure [7,8]. Currently, the synthesis of peptoids is complex and time-consuming but strategies for controlling the processes' efficiency and scale are proceeding quickly [9].

Among the various materials for implants, titanium and its alloys are frequently used, mostly in dental and orthopedic implants, for their high osseointegration ability and biocompatibility. Because titanium is an example of bioinert material, scientific research has focused on topographic and surface modification as a means of making the implant bioactive, stimulating and accelerating the osseointegration process. The titanium alloys can become bioactive with proper chemical etchings and, in this way, the precipitation of the mineral component of the bone (hydroxyapatite) occurs on the surface from the physiological fluids [10]. Physic-chemical properties of an implant surface such as topography, wettability, roughness, and surface potential regulate the protein adsorption and cell adhesion [11,12]. In particular, the topographical texture of implant surfaces has an important role in tissue response. Surface topography is fundamental for the adhesion and differentiation of osteoblasts in the initial stage of osseointegration. This is why micro- and nano-scale rough surfaces have greater surface area for tissue integration than smooth surfaces and increase the number and strength of focal adhesions (bone on-growth). Nanoscale roughness with size in the magnitude of protein and cell membrane receptors dimensions could also act in cell adhesion, proliferation, and spreading [13–15].

AMPs are often conjugated with metal biomaterials, particularly titanium, to impart antibacterial properties to implant surfaces. Functionalization of AMPs on titanium surfaces can be achieved through various methods, such as covalent bonding [16–28,28–30], or physical adsorption [31–33]. Once the AMPs are functionalized on the titanium surface, they can provide a potent antimicrobial barrier against bacterial infections. Despite the rich literature on AMPs functionalized on titanium, there are still no cases where peptoids are used for surface functionalization. The feasibility and advantages of the functionalization of titanium surfaces with peptoids are still to be proven.

In this work, a peptoid (GN2-Npm$_9$ – Fig. 1), rich in lysine and tryptophan-like residues, was synthesized using a Solid Phase Synthesis protocol (SPS). Preliminary studies reported the ability of this peptoid to inhibit the growth of *E. Coli,* by disrupting its membrane integrity [34–37]. So, here the peptoid's antibacterial efficacy has been exploited to prevent the infection of implantable titanium as a potential alternative to common strategies. In addition, GN2-Npm$_9$ was carefully chosen has a good candidate for its low cytotoxicity.(IC$_{50}$ 104 μg/ml) compared with other synthesized peptoids [36]. For these reasons, GN2-Npm$_9$ here it was used to
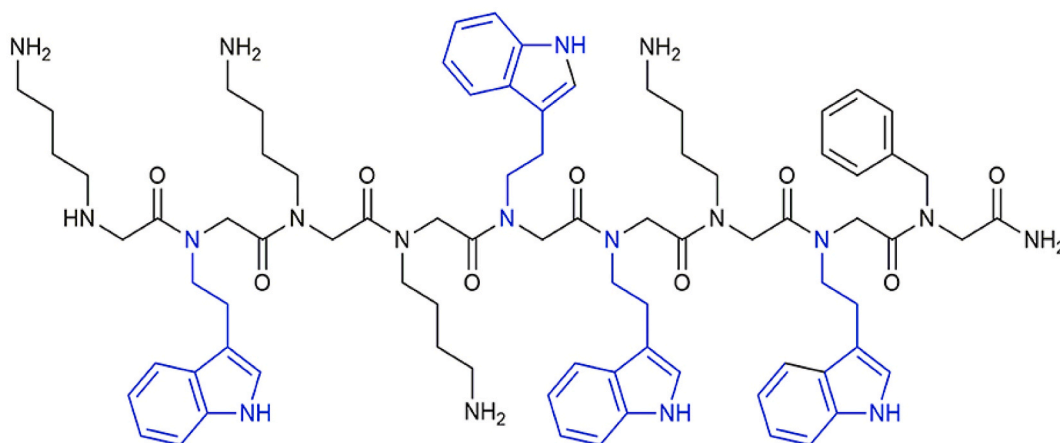

Fig. 1. *The chemical structure of GN2-Npm$_9$ peptoid* [39].

functionalize a chemically pre-treated Ti6Al4V surface for permanent implant application.

The surface obtained after the chemical pre-treatment displays both micro-and nano-roughness (Ra = 0.25 μm), and exposes a chemically modified titanium oxide layer with acidic OH groups that allow not only pro-osteogenic properties but make the substrate suitable for grafting and functionalization with biomolecules [38].

This study aimed to develop a biocompatible and antibacterial surface by GN2-Npm$_9$ functionalization. To the extent of our knowledge, no work combines a synthetic peptoid with titanium alloy. The surface functionalization process of the chemically pre-treated Ti6Al4V (CT) with the peptoid has been optimized, by chemisorption on the surface, exploiting the electrostatic attraction between the peptoid, which is positively charged at physiological pH, and the chemically pre-treated surface. A preliminary physical-chemical characterization of the obtained surface was carried out with zeta potential titration curves and contact angle measurements. Finally, the antibacterial action performance of the functionalized surfaces was assessed towards the *S. Epidermidis and E. Coli* showing promising anti-biofilm activity, while cytocompatibility evaluation was verified on mesenchymal stem cells (hMSc)

2. Materials and methods

2.1. Peptoid synthesis

GN2-Npm$_9$ was synthesized using solid-phase Fmoc chemistry with amidation at the carboxyl end (MHBA resin-loading capacity 0,65 mmol/g) and purified by reversed-phase HPLC using a C18 column (Higgins Analytical Inc. 10 μm 250 × 10 mm) and a water/acetonitrile gradient. The correct mass and purity >95 % were verified by Dionex Ultimate 3000 RP-UHPLC (C18 Kinetex 100 × 2.1 mm, 100 Å) electrospray ionization mass spectrometry (Finnigan LTQ).

2.2. Surface pre-treatment

The substrate chosen for the surface modifications is titanium alloy Ti6Al4V (ASTM B348, Gr5, Titanium Consulting and Trading, 10 mm diameter discs). All discs were polished with SiC paper (up to 400 grit). To clean the surface, the samples were first immersed in acetone for 5 min and then twice for 10 min in high-purity Milli-Q (MQ, Millipore) water in an ultrasonic bath. The samples were subjected to a patented chemical treatment [40] involving initial acid etching in dilute hydrofluoric acid followed by controlled reoxidation with hydrogen peroxide. Before functionalization, the treated samples were irradiated with UV light for 1 h to reduce the water content and carbon impurity and to improve the reactivity of the hydroxyl groups. From now on, the samples treated as described above will be referred to as chemically pre-treated (CT), while the samples polished to a grain size of 4000, which served as a control, will be referred to as mirror polished (Ti64).

2.3. Surface functionalization

A solution of PBS and 1 mg/mL GN2.Npm$_9$ was previously prepared by stirring the molecule in PBS for 5 min and then filtering through a 0.2μ filter to leach out bacterial contamination. With the solution prepared, the CT samples were withdrawn from UV irradiation and placed on a Petri dish. A 100-μl drop of the solution was dropped onto the sample so that the entire surface of the sample was covered, taking care not to break the drop. The samples were left in an incubator at 37 °C for 2 h. The samples were then rinsed in double distilled water to remove the non-adherent peptoid on the surface and dried under a hood. The functionalized samples were denoted as CT_GN2-Npm$_9$. Control samples (CT_PBS) were prepared with the same procedure, without adding the molecule (GN2-Npm$_9$) in PBS.

2.4. Zeta potential measurements on solid sample

The zeta potential titration curves were measured by an electrokinetic analyzer (SurPASS, Anton Paar GmbH, Graz, Austria) for both functionalized and non-functionalized samples and control samples (CT_GN2-Npm$_9$, CT, and CT_PBS). The zeta potential was determined as a function of pH in an electrolyte solution of 0.001 M KCl, and the pH value (which starts at approximately 5.5) was varied by adding 0.05 M HCl or 0.05 M NaOH using the automatic titration unit of the instrument. The isoelectric point (IEP) was established as the intercept of the titration curve with the x-axis (zeta potential = 0 mV). Two different sets of samples were used for each basic and acid curve. The expected IEP values of the monomers were calculated by using BACHEM software for peptides calculation (https://www.bachem.com/knowledge-center/peptide-calculator/2).

2.5. Contact angle measurements

Surface wettability was assessed by measuring the contact angle with the sessile drop method. After depositing a 10 μl drop of water on the treated side of the sample, the contact angle was measured through Image J software after acquiring images with a microscope (Kruss DSA 100). The contact angle was measured on CT, CT_GN2-Npm$_9$, and CT_PBS.

2.6. Zeta potential measurement on liquid sample

The Zeta potential of an aqueous solution with the peptoid at a concentration of 1 mg/ml was measured with the Litesizer 500

particle analyzer (Anton Paar), using Smoluchowski as an approximation formula, and a debye factor of 1.5. Titration was done manually adjusting the pH with NaOH 0.005 M and HCl 0.005 M.

2.7. Biological evaluation

2.7.1. Cytocompatibility evaluation

Specimens were sterilized by UV-light exposure (30 min) before biological experiments. To test specimens' cytocompatibility, human bone marrow-derived stem cells (hMSC) were obtained from Merck (Promo Cell C-12974) and cultivated in low-glucose Dulbecco's modified Eagle Medium (DMEM, Merck) supplemented with 15 % fetal bovine serum (FBS, Merck) and 1 % antibiotics (penicillin/streptomycin, Merck) at 37 °C, 5 % CO_2 atmosphere. Cells were cultivated until 80–90 % confluence, detached by a trypsin-EDTA solution (0.25 % in PBS, from Merck), harvested, and used for the experiments.

Cells were directly dropwise seeded onto the specimens' surface at a defined concentration (2.5×10^4 cells/specimens) and cultivated for 1 and 2 days. At each time-point, the viability of the cells has been deduced in the function of their metabolic activity by the colorimetric assay alamar blue (alamarBlue™, ready-to-use solution from Invitrogen™) following manufacturer's instructions. Accordingly, fluorescence signals were evaluated with a spectrophotometer (Spark®, Tecan Trading AG, CH) using an excitation wavelength of 570 nm and a fluorescence emission reading of 590 nm. Results are expressed in relative fluorescence units (RFU). Untreated mirror-polished Ti specimens were considered as a positive control (100 % viability).

To verify cells' spread and confluence onto specimens' surface, on day 2 specimens were washed with PBS, fixed with 4 % paraformaldehyde (20 min, room temperature), permeabilized for 20 min with Triton (0.5 % in PBS), and then stained with Texas Red™-X Phalloidin (Thermo Scientific; Invitrogen: T7471) and 4,6-diamidino-2-phenylindole (DAPI, Sigma, Aldrich) to visualize f-actins cytoskeleton filaments and nuclei, respectively. Images were collected by a confocal microscope (Leica SP8 confocal platform, Leica Microsystems, Germany).

Scanning electron microscopy (SEM) was applied to better appreciate the adaptation of cells to the surfaces' morphology. Accordingly, cells were fixed with 2.5 % glutaraldehyde, dehydrated by the alcohol scale (50 %, 70 %, 90 %, and 100 %, 2 h each), and finally treated with hexamethyldisilazane (from Alfa Aesar, Waltham, MA, USA). Then, specimens were mounted onto aluminum stubs, surface metalized by gold, and observed with an SEM-EDS JEOL JSM-IT 500.

2.7.2. Antibacterial properties

Specimens' ability to prevent surface bacterial infection was verified towards the Gram-positive *Staphylococcus epidermidis (S. epidermidis)* and the Gram-negative *Escherichia coli (E. coli)* pathogens. Strains were obtained from the American Type Culture Collection (*S. epidermidis* ATCC 14990, *E. coli* ATCC 25922) and cultivated following the manufacturer's instructions. Fresh broth cultures were prepared before each experiment to test bacteria in their exponential growth phase. The final number of bacteria was adjusted to 1×10^5 bacteria/ml by optical density (0.001 at 600 nm).

Specimens' infection was performed according to the ISO 22196 standard. So, an aliquot of 100 μl of the above-mentioned bacterial suspensions was gently seeded onto the specimens' surface, covered with a sterile polyethylene film, and placed in an incubator at 35 °C for 24 h. Then, the cover film was gently removed, specimens were washed 3 times with PBS to remove non-adherent bacteria, and alamar blue was applied to determine bacterial viability in the function of the metabolic activity as prior detailed. Moreover, SEM imaging was applied to check the formation of biofilm-like 3D aggregates in the function of the surfaces' properties.

2.7.3. Selectively targeted activity

Specimens' ability to preserve cells from infection was evaluated by a cell-bacteria co-culture assay as prior reported by the authors [41]. Briefly, 2.5×10^4 cells/specimen of hBMSC were seeded onto the specimens' surface and allowed to adhere and spread for 24 h. The day after, after excluding the presence of apoptotic cells floating into the medium or wrongly adhered to the plastic, specimens were infected with 1 ml of antibiotics-free DMEM containing 1×10^3 *S. epidermidis* colonies. After 48 h of infection, specimens were collected, washed carefully 3 times with PBS and surface-adhered cells and bacteria were detached by trypsin digestion. Viable cells were counted by a Bürker chamber and trypan blue stain to determine the viable number, while bacteria were evaluated by the colonies forming unit (CFU) by seeding them into Luria Bertani semi-solid agar plates after serial dilutions [42].

2.8. Statistical data analysis

Biological evaluations were performed using technical triplicates. Results were analyzed by using SPSS software (v25, IBM, New York City, NY, USA) and one-way ANOVA followed by Tukey's test as post hoc analysis. The significance level was set at $p < 0.05$.

3. Results and discussions

A characterization of CT is already reported in previous works [38,43] The focus of this paper was on CT_GN2-Npm$_9$, and data about CT as a control sample are here reported when needed.

3.1. Zeta potential measurements

Fig. 2 displays the titration curves of the CT, CT_PBS, and functionalized samples (CT, CT_GN2-Npm$_9$). In the same figure, the

titration curve of a solution of GN2-Npm$_9$ is also reported. At a glance, the curve of CT_GN2-Npm$_9$ appears considerably different from that of control samples (CT and CT_PBS) confirming the effectiveness of the functionalization process. This is the first key information from this measurement.

CT and CT_PBS have the same titration curves, suggesting that the immersion of CT in PBS did not change its surface chemistry. The CT curve had an IEP at a very low pH ($\approx$3), a low slope in the acid range of the titration with a change of the slope at pH 4, and a stable plateau (at around -45 mV) in the basic range, with an onset at pH 5.5. These features were due to the CT surface's chemistry [44]. The CT sample, after undergoing the chemical pre-treatment, acquired a hydrophilic surface with a titanium oxide layer and high density of OH groups. The hydroxyl groups were exposed and exhibited a highly acidic behavior, being deprotonated at pH as low as 3–5.5. An IEP at around 4 is expected for a surface without acidic/basic functional groups or a balance of them, while a shift towards lower values is expected in the presence of acidic functional groups. The prevalence of the negatively charged OH functional groups on the surface induced the low IEP of CT and a negative charge of the surface for all pH range, even at physiological pH. This feature makes CT a bioactive material. CT surface attracts Ca^{2+} ions from the physiological fluids and induces the in-vivo precipitation of hydroxylapatite (bioactivity) [38,57]. Water molecules adhered firmly to the hydrophilic CT surface and were not easily replaced by ions in the solution as the pH changed. This was the origin of the low slope of the curve in the acidic range of the titration. A plateau resulted from OH groups being completely deprotonated at pH values higher than 5.5.

The zeta potential titration curve of a solution of the peptoid GN2-Npm$_9$ (Fig. 2) shows an isoelectric point around 9.5 and a positive zeta potential in all the explored range of pH. This curve can be explained considering its chemical structure. Lysine has an IEP of 9.7, the pKa of the alpha carboxylic group is 2.2, that of the ammonium group is 8.9, and that of the side chain is 10.5 [45]. Tryptophan has an IEP of 5.9, the pKa of the alpha carboxylic group is 2.5, and that of the ammonium group is 9.4. It has an apolar and hydrophobic side chain. The here used tryptophan-like residue is expected to be similar. The IEP of the dipeptide and polypeptides lysine-tryptophan was expected to be around pH 10 because carboxylic groups were engaged into the peptide bond, by adding more units, and were not available for deprotonation, while the number of the basic side chain of lysine were available for protonation. The titration curve was not expected to change by changing the sequence of the monomers inside the chain.

The IEP of the functionalized surface CT_ GN2-Npm$_9$ shifted towards more basic values vs CT, reaching a pH around 6, which confirmed the presence of the adsorbed peptoid on the CT substrate but without a complete coverage of the surface because the IEP of GN2-Npm$_9$ was not reached. The shape of the curve of CT_GN-Npm$_9$ can be explained as due both to the functionalities of CT and GN2-Npm$_9$. The positive zeta potential at pH 3–4 was likely due to the exposure of the positive surface charges (amine groups) of the peptoid. A plateau of the zeta potential was observed around pH 4–5.5 because of the deprotonation of the OH groups of CT not covered by the peptoid. Then, the high slope of the curve at pH 5.5–9 was due to the apolar and hydrophobic side chain of the tryptophan-like residue. It could be assumed that the hydrophilic residues of GN2-Npm$_9$ (lysine) were attracted by the substrate surface and were facing it, while the hydrophobic ones (tryptophan-like) were facing the solution.

At the pH value chosen for the functionalization process (pH = 7.4), the CT substrate had a negative surface charge with completely deprotonated –OH groups, whereas GN2-Npm$_9$ had an overall positive charge. Based on these conditions, an electrostatic attraction between the substrate and the peptoid, resulting in a chemisorption mechanism, could be predicted.

3.2. Contact angle measurement

Fig. 3 illustrates the water contact angles measured on a surface-functionalized sample (CT_GN2-Npm$_9$), and two reference samples: CT and CT_PBS. A protocol analogous to CT_GN2-Npm$_9$ was used to prepare CT_PBS but without the addition of GN2-Npm$_9$ to the
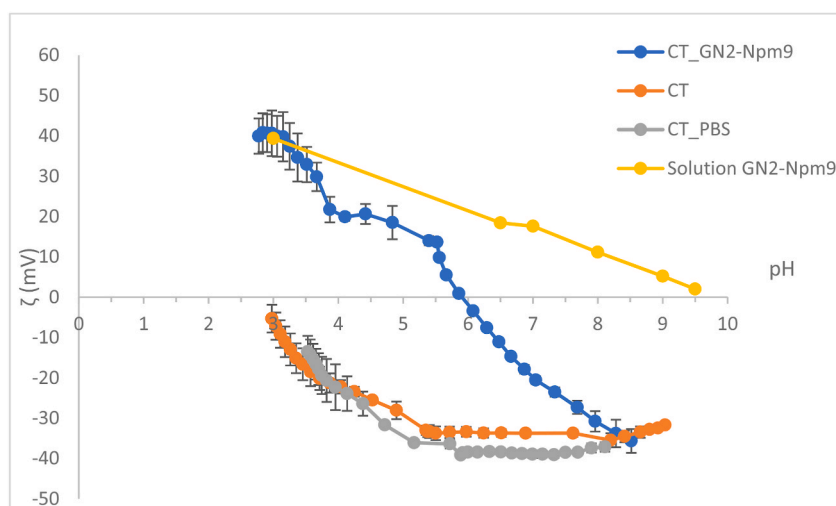
Fig. 2. potential titration curve of CT, CT_PBS, CT_GN2Npm$_9$ and GN2-Npm$_9$ solution

solution. The CT sample exhibited a contact angle of approximately 40°, as supported by the zeta potential curve and the expected high density of OH groups, making the surface more hydrophilic compared to Ti64 sample's surface which exhibit a higher contact angle of approximately 65°. CT_PBS sample had a contact angle of approximately 5°. The exact origin of the high hydrophilicity of this control sample is not completely clear, but it lies outside the scope of this paper. Comparing the CT_PBS and CT_GN2-Npm$_9$ samples, the presence of the adsorbed peptoid was confirmed by the different contact angles. Thus, it can be inferred that the CT_GN2-Npm$_9$ sample exhibited a hydrophilic behaviour but the exposure of GN2-Npm$_9$ (exposing hydrophobic moieties) significantly increased the contact angle vs CT_PBS, reaching values of approximately 25°, which was statistically different from both the controls ($p < 0.05$). Surface roughness can affect the wettability of a surface together with its chemistry. The measured roughness of CT (Ra = 0.25 μm) did not increase the real surface area [46]and it is not expected to significantly affect wettability. Moreover, zeta potential titration curve is not sensitive to roughness but showed an evident hydrophilic behaviour of CT. In conclusion, a major role of chemistry on wettability of these samples is expected. In the case of CT and GN2-Npm$_9$ From the perspective of an implant, surface wettability is important as it affects cell adhesion and well-being. It has been found that a surface suitable for cell adhesion is a hydrophilic surface with contact angles ranging from 30 °C to 65 °C and above 40 mN/m in terms of surface energy [47,48].

3.3. Biological evaluation

3.3.1. Cytocompatibility evaluation

Cytocompatibility evaluation was performed on mesenchymal stem cells as they represent a frequent and consolidated pattern to test *in vitro* the ability of an implantable device to support the recruitment and colonization from the progenitor cells migrating towards the injured site. The bulk titanium alloy (Ti64) has been considered a positive control due to the large literature, including clinical revisions, suggesting its biocompatibility and successful osteointegration after months upon implantation [49,50]. Accordingly, it has been considered as 100 % viability to rank the results coming from CT and CT_GN2-Npm$_9$ specimens. Results are reported in Fig. 4.

In general, the presence of the peptoid did not impair the ability of the hMSC to colonize specimens' surface, thus being metabolically active at both 1 or 2 days after seeding as demonstrated by the Alamar blue assay (Fig. 4a) where the reported RFU were not significantly reduced comparing CT and CT_GN2-Npm$_9$ with the Ti64 control ($p > 0.05$). So, the percentage of viable cells was always >90 % as reported in Fig. 4b. As a confirmation of the presence of viable cells, SEM imaging (Fig. 4c) showed that cells were able to adapt to the CT_GN2-Npm$_9$ surface similarly to the untreated Ti64 controls reporting a similar morphology despite the presence of the functionalized layer and the microtopography due to CT pre-treatment. Fluorescence staining of cells' cytoskeleton and nuclei (Fig. 4d) provided further evidence of the cell-friendly behavior of the test CT_GN2-Npm$_9$ surfaces. In particular, the density of the DAPI-stained nuclei demonstrated a comparable cellular confluence between the Ti64 control and CT_GN2-Npm$_9$ thus confirming the ability of the test specimens to support the colonization of progenitor cells, albeit with all the limitations relating to an *in vitro* experiment.

In general, ranking our results in comparison to previous works is not easy due to the large variety of synthesized peptoids available in the current literature. However, some articles report on peptoids' cytocompatibility and bioactivity toward mesenchymal stem cells. As an example, Morton et al. exploited unstructured, helical, and non-helical peptoids to tune the biomechanical properties of hydrogels to realize 3D cultures of stem cells that did not report any toxic effect after seeding and cultivating in direct contact [51]. Statz et al. were able to correlate the length and the surface density of peptoids on titanium substrates with their antifouling activity towards fibroblasts. Results showed that cells' adhesion can be prevented by reducing pro-adhesion protein surface accumulation but toxic effects due to the peptoids coating were not reported [52]. Similarly, Zhao et al. reported the use of peptoid-loaded microgels as a bioactive coating to prevent bacterial contamination of Ti substrates in a simulated surgery infection model reporting that such treatment was not toxic toward human progenitor fetal osteoblasts that were used as cells deputed to drive the implant colonization [53].

So, our results seem to be in line with previous literature suggesting the use of the GN2-Nmp$_9$ peptoid as a cytocompatible tool to coat biomedical Ti substrates.
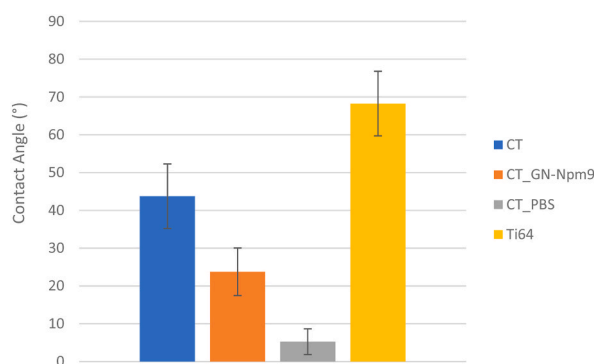

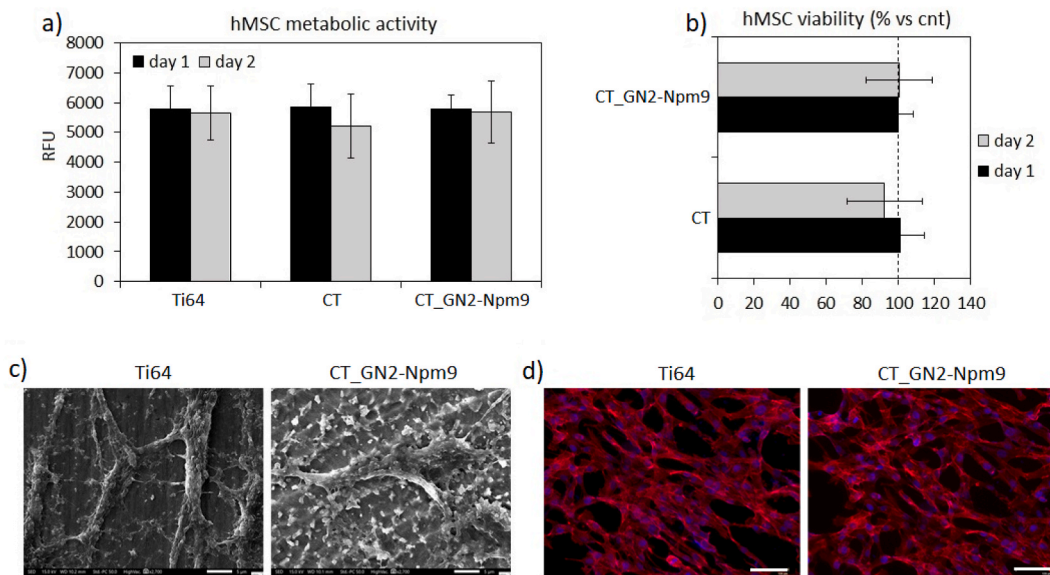**Fig. 3.** Contact angle of CT, CT_GN2-Npm$_9$, CT_PBS and Ti64

Fig. 4. Cytocompatibility evaluation of CT, Ti64, and CT_GN2-Npm$_9$ (a) Cells seeded onto peptoid-doped surfaces (CT_GN2-Npm$_9$) reported a comparable metabolic activity in comparison to the Ti64 control and the CT ones (p > 0.05). (b) Accordingly, the viability ranged between 90 and 100 % in comparison with Ti64 controls. (c) SEM images confirmed the ability of cells to adapt onto the CT_GN2-Npm$_9$ surface as well as (d) fluorescent staining demonstrated a comparable cell density between test and control specimens. Bars represent mean±sdev.st; replicates n = 3. SEM bar scale = 5 μm (2700x); fluorescence bar scale = 125 μm

3.3.2. Antibacterial properties

Orthopedic implant infection represents a huge clinical burden strongly reducing the patient's quality of life due to the frequent need to remove infected devices [54]. Therefore, there is an urgent need to develop new strategies conferring antibacterial properties to the materials aimed for implantation to prevent bacterial infections thus avoiding further surgeries.

In this direction, peptoids have been reported to represent an attractive tool as many proofs about their antibacterial properties have been provided by the literature [55,56]. So, here the GN2-Nmp$_9$ peptoid was exploited to coat the surface of the CT chemically pre-treated surfaces to combine the peptoids' bioactivity and the nanostructured surface topography of the specimens, considering that such peptoid was previously reported to efficiently determine *E. coli* death by membrane irreversible destruction (MIC = 16 μg/mL) [34].

Accordingly, specimens were infected with *S. epidermidis* (Gram-negative) and *E. coli* (Gram-positive). These strains were selected because they are often involved in orthopedic infections and to test the antibacterial efficacy of the peptoids against both the Gram species. The results are reported in Fig. 5.

In general, the CT nano-topography reduced the metabolic activity of both pathogens but only *E. coli* was significant in comparison with Ti64 controls (Fig. 5 ac, p < 0.05 indicated by #). As previously shown by the authors, this effect is due to the needle-like nanostructures formed after the chemical pre-treatment that can directly cause bacteria death by irreversible membrane damage thus preventing proliferation or by preventing their adhesion by reducing the anchorage sites in the early adhesion phase [57,58]. So, this was a predictable difference as the Gram-positive strains are expected to be more sensitive to the surface morphology due to the membrane thickness and the relative difficulty of modifying the cytoskeleton based on topography. However, the presence of the peptoid significantly improved the ability of the CT specimens to further reduce the colonization in comparison with the CT per-se (Fig. a,c indicated by the §). In fact, CT_GN2-Npm$_9$ resulted as significant towards both Ti64 control and CT for *S. epidermidis* and *E. coli* (Fig. 5a–c), thus confirming their antibacterial and broad-range activity. As a consequence, bacterial viability was reduced by ~ 77 % for *S. epidermidis* (Fig. 5b) and by ~ 89 % for *E. coli* (Fig. 5d). Accordingly, it can be hypothesized that also those bacteria being able to adapt to the nano-topography of the CT specimens were prevented from proliferation by the presence of the peptoid onto the surface that bonded to the bacteria membranes after surface colonization.

Finally, SEM images (Fig. 5e, representative of the *S. epidermidis* strain) validated the results obtained by the metabolic assay. While Ti64 reported a highly colonized surface with bacteria aggregated into dense and thick biofilm-like 3D structures, only a few colonies mostly arranged in small aggregates were observed on CT_GN2-Npm$_9$ specimens.

So, our results confirmed the antibacterial activity provided by the peptoids that significantly improved the preventive antifouling and antiadhesive effect due to the CT nano-topography. Such a synergistic effect can be expected since the mechanism underlying the antibacterial effect of peptoids is different from the membrane rupture caused by the needle-like effect of the nano-topography. Amine residues with a positive electrostatic charge allow a strong bond between GN2-Nmp$_9$ and the bacterial membrane. Such interaction brings in the formation of irreversible pores in the membrane causing bacterial death due to the loss of the balanced homeostasis affected by the intra/extra-cellular trafficking of ions and nutrients [59]. Accordingly, the authors hypothesize that the strong
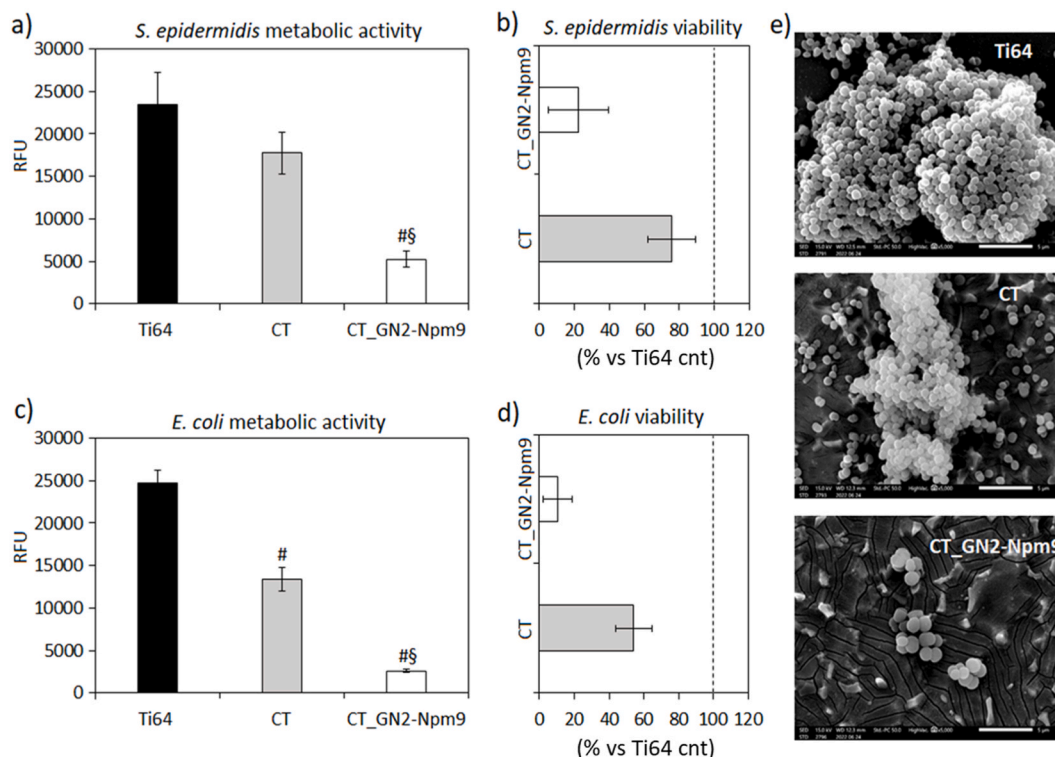
Fig. 5. Antibacterial properties of CT, Ti64, and CT_GN2-Npm9. The nano-topography of the CT specimens determined a significant reduction of E. coli metabolic activity (c, p < 0.05 indicated by #) but only the introduction of peptoids significantly decreases bacterial metabolic activity in comparison to both Ti64 controls (a-c, p < 0.05 indicated by #) and CT (a-c, p < 0.05 indicated by §). This led to a reduction of bacterial viability ranging between 70 and 90 % in comparison with Ti64 controls (b–d). SEM images confirmed the strong reduction of colonies into the CT_GN2-Npm9 surfaces as well as the prevention of dense 3D biofilm-like aggregates (e, representative for S. epidermidis). Bars represent mean±sdev.st; replicates n = 3. SEM bar scale = 5 μm (5000x).

antibacterial effect observed on CT_GN2-Nmp9 can be ascribed to the synergistic activity of the reduced bacterial adhesion due to the CT nano-topography combined with the disruptive effect of the peptoid towards the bacterial membrane.

Lastly, as the authors already described in previous findings related to the antimicrobial peptide Nisin [60,61], the functionalization through a chemisorption mechanism is advantageous both in comparison with physisorption, which is a weak and poorly controlled bond with the surface, and covalent grafting, that does not allow the release of the antibacterial agent (such as the peptoid, in this case), resulting in a weak antibacterial effect.

3.3.2.1. Selectively targeted activity. After demonstrating CT_GN2-Npm9 specimens' cytocompatibility and antibacterial activity, bacteria-cells co-cultures were used to verify whether the antibacterial effect was targeted to preserving cells' viability in an environmental competition between hMSC and *S. epidermidis* [41,62]. It must be considered that cells and bacteria are not separate entities in the real clinical scenario, but, on the contrary, they compete to adhere and colonize the same surface (in this case the newly implanted biomedical device) putting in place a sort of "race for the surface" [63].

Results are reported in Fig. 6. In general, such experiments confirmed previous findings related to antibacterial and cytocompatibility studies. In fact, in the absence of any antibacterial agent, bacteria adhered, proliferated and infected the Ti64 controls thus reducing the number of viable cells colonizing the surface. The number of viable cells decreased by ≈ 47 % (Fig. 6 a) in comparison to the seeded number, while, on the contrary, the number of bacteria increased by > 2 logs (Fig. 6b) compared to the early stage of the infection. SEM images (Fig. 6c) confirmed the presence of bacterial aggregates (indicated by the red circle) in proximity to apoptotic cells (indicated by the black arrows). According to the previous findings related to the antibacterial studies (Fig. 5), the results obtained by the Ti64 specimens were considered to rank the CT and CT_GN2-Npm9 as it was demonstrated that untreated specimens were not able to counteract bacterial infection. So, CT specimens reported mostly a bacteriostatic effect since the number of viable bacteria increased only by < 1 log (Fig. 6b) and the number of viable cells was increased compared to the Ti64 control (Fig. 6a). SEM images reported the presence of cells with a proper morphology, but also the accumulation of biofilm aggregates overhanging cells' cytoskeleton (indicated by the red circles). Those results can be expected. As it was previously discussed, nano-topography is a physical hurdle for bacteria during the adhesion phase and a cause of membrane rupture in the proliferation stage. Finally, the presence of the peptoid chemisorbed on the CT surface was effective in reducing the number of viable bacteria of ≈1 log (Fig. 6b) as well as the number of cells increased by ≈ 17 % compared to the seeded number. SEM images (Fig. 6c) confirmed the presence of cells
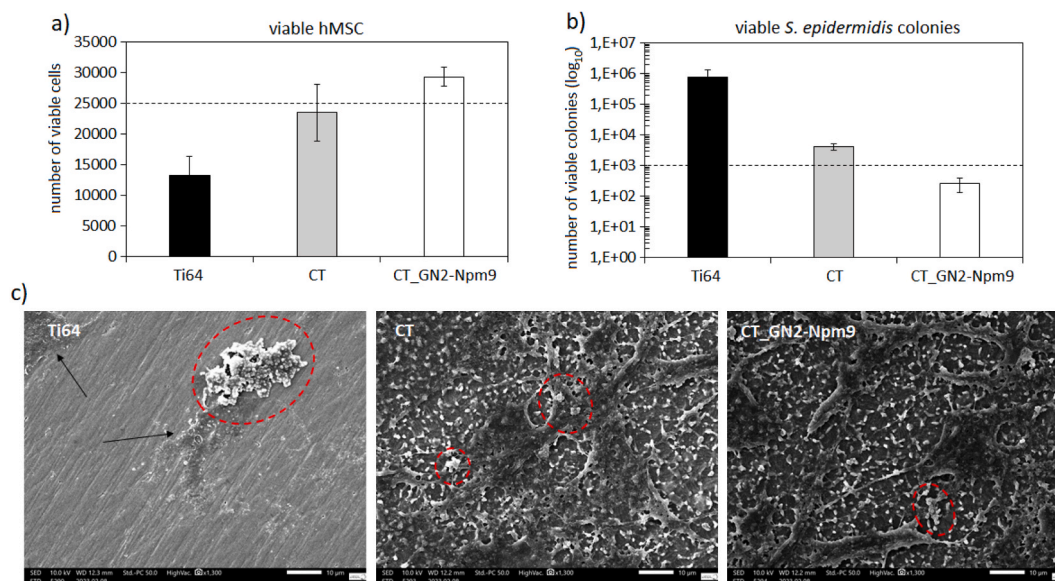
Fig. 6. Peptoid's selective targeted activity. The peptoid doping allowed for a parallel increase of the cells seeded onto the surface (a, the dashed line indicates the starting number of cells) and a decrease of bacteria colonizing the surface (b, the dashed line indicates the starting number of bacteria) in this competition model. SEM images c) demonstrated that onto Ti64 surfaces biofilm-like bacteria aggregates were visible (indicated by the red circles) and cells appeared as degraded (indicated by the arrows), while onto CT_GN2-Npm9 ones cells were intact and homogeneously distributed while only few single bacteria were visible. Bars represent mean±sdev.st; replicates n = 3. SEM bar scale = 10 μm (1300x).

displaying regular morphology and only a few bacterial colonies mostly in a single conformation rather than in the biofilm-like 3D arrangement which appears not to interact with cells.

So, coming back to the basic hypothesis of the co-culture experiment, it can be speculated that the CT_GN2-Npm$_9$ surfaces are a very promising combination of nano-topography and adsorbed bioactive compound selectively preventing bacterial infection while preserving cells' ability to colonize the device. Further studies are still necessary to confirm specimens' properties for tissue engineering applications in a more biologically rich in vivo environment where other factors such as blood proteins surface accumulation can change the scenario. A more in-depth physical-chemical analysis is required to better understand the orientation of the adsorbed peptide on the surface and image its distribution on the surface, whether homogenous or not. The study of the release kinetics is also required to study how and whether the peptoid is released from the surface.

4. Conclusion

In this work, the antimicrobial peptoid GN2-Npm$_9$ was used to functionalize a chemically pre-treated Ti6Al4V alloy (CT). A preliminary physical-chemical characterization (zeta potential titration and contact angle measurements) of CT_GN2-Npm$_9$ showed a hydrophilic surface, suitable for cell proliferation and adhesion, and an effective functionalization through a chemisorption mechanism. Biological tests showed a strong antibacterial activity without any cellular cytotoxicity even when cells and bacteria competed in a co-culture. The functionalized surface was a very promising combination of nano-topography and adsorbed peptoid selectively preventing bacterial infection while preserving cells' ability to colonize the device for permanent bone contact applications.

Additional information

No additional information is available for this paper.

CRediT authorship contribution statement

Francesca Gamna: Writing - review & editing, Writing - original draft, Methodology, Investigation, Data curation, Conceptualization. **Andrea Cochis:** Writing - review & editing, Writing - original draft, Methodology, Investigation, Data curation. **Biljana Mojsoska:** Writing - review & editing, Validation, Investigation, Data curation. **Ajay Kumar:** Investigation. **Lia Rimondini:** Validation, Supervision. **Silvia Spriano:** Writing - review & editing, Writing - original draft, Validation, Supervision, Conceptualization.

Declaration of competing interest

The authors declare that they have no known competing financial interests or personal relationships that could have appeared to

influence the work reported in this paper.

References

[1] R. Boöttger, R. Hoffmann, D. Knappe, Differential stability of therapeutic peptides with different proteolytic cleavage sites in blood, plasma and serum, PLoS One 12 (6) (2017) 1–15, https://doi.org/10.1371/journal.pone.0178943.

[2] K.L. Zapadka, F.J. Becher, A.L. Gomes dos Santos, S.E. Jackson, Factors affecting the physical stability (aggregation) of peptide therapeutics, Interface Focus 7 (6) (2017), https://doi.org/10.1098/rsfs.2017.0030.

[3] D. Psimadas, P. Georgoulias, V. Valotassiou, G. Loudos, Molecular nanomedicine towards cancer, J. Pharm. Sci. 101 (7) (2012) 2271–2280, https://doi.org/10.1002/jps.

[4] C. Adessi, C. Soto, Converting a peptide into a drug: strategies to improve stability and bioavailability, Curr. Med. Chem. 9 (9) (2005) 963–978, https://doi.org/10.2174/0929867024606731.

[5] F. Pucci, R. Bourgeas, M. Rooman, Predicting protein thermal stability changes upon point mutations using statistical potentials: introducing HoTMuSiC, Sci. Rep. 6 (February) (2016) 1–9, https://doi.org/10.1038/srep23257.

[6] A. Saini, G. Verma, Peptoids: Tomorrow's Therapeutics, Elsevier Inc., 2017.

[7] J. Sun, R.N. Zuckermann, Peptoid polymers: a highly designable bioinspired material, ACS Nano 7 (6) (2013) 4715–4732, https://doi.org/10.1021/nn4015714.

[8] M.T. Dohm, R. Kapoor, A.E. Barron, Peptoids: bio-inspired polymers as potential pharmaceuticals, Curr. Pharmaceut. Des. 17 (25) (2012) 2732–2747, https://doi.org/10.2174/138161211797416066.

[9] A.M. Clapperton, J. Babi, H. Tran, A field guide to optimizing peptoid synthesis, ACS Polym. Au 2 (6) (2022) 417–429, https://doi.org/10.1021/acspolymersau.2c00036.

[10] H.M. Kim, F. Miyaji, T. Kokubo, T. Nakamura, Preparation of bioactive Ti and its alloys via simple chemical surface treatment, J. Biomed. Mater. Res. 32 (3) (1996) 409–417, https://doi.org/10.1002/(SICI)1097-4636(199611)32:3<409::AID-JBM14>3.0.CO;2-B.

[11] A. Hasan, L.M. Pandey, Surface Modification of Ti6Al4V by Forming Hybrid Self-Assembled Monolayers and its Effect on Collagen-I Adsorption, in: Osteoblast Adhesion and Integrin Expression, vol. 505, Elsevier B.V., 2020.

[12] A. Hasan, V. Saxena, L.M. Pandey, Surface Functionalization of Ti6Al4V via Self-assembled Monolayers for Improved Protein Adsorption and Fibroblast Adhesion 34 (11) (2018).

[13] R. Krishna Alla, K. Ginjupalli, N. Upadhya, M. Shammas, R. Krishna Ravi, R. Sekhar, Surface roughness of implants: a review, Trends Biomater. Artif. Organs 25 (3) (2011) 112–118.

[14] D.N.R. Vootla, D.K.V. Reddy, Osseointegration- key factors affecting its success-an overview, IOSR J. Dent. Med. Sci. 16 (4) (2017) 62–68, https://doi.org/10.9790/0853-1604056268.

[15] S. Parithimarkalaignan, T.V. Padmanabhan, Osseointegration: an update, J. Indian Prosthodont. Soc. 13 (1) (2013) 2–6, https://doi.org/10.1007/s13191-013-0252-z.

[16] F.M.T.A. Costa, S.R. Maia, P.A.C. Gomes, M.C.L. Martins, Dhvar5 antimicrobial peptide (AMP) chemoselective covalent immobilization results on higher antiadherence effect than simple physical adsorption, Biomaterials 52 (1) (2015) 531–538, https://doi.org/10.1016/j.biomaterials.2015.02.049.

[17] L. Zhou, et al., Biofunctionalization of microgroove titanium surfaces with an antimicrobial peptide to enhance their bactericidal activity and cytocompatibility, Colloids Surf., B 128 (2015) 552–560, https://doi.org/10.1016/j.colsurfb.2015.03.008.

[18] B. Nie, H. Ao, J. Zhou, T. Tang, B. Yue, Biofunctionalization of titanium with bacitracin immobilizationshows potential for anti-bacteria, osteogenesis and reduction ofmacrophage inflammation, Colloids Surf., B 145 (2016) 728–739, https://doi.org/10.1016/j.colsurfb.2016.05.089.

[19] B. Nie, H. Ao, T. Long, J. Zhou, T. Tang, B. Yue, Immobilizing bacitracin on titanium for prophylaxis of infections and for improving osteoinductivity: an in vivo study, Colloids Surf., B 150 (2017) 183–191, https://doi.org/10.1016/j.colsurfb.2016.11.034.

[20] K.V. Holmberg, M. Abdolhosseini, Y. Li, X. Chen, S.U. Gorr, C. Aparicio, Bio-inspired stable antimicrobial peptide coatings for dental applications, Acta Biomater. 9 (9) (2013) 8224–8231, https://doi.org/10.1016/j.actbio.2013.06.017.

[21] P. Siwakul, L. Sirinnaphakorn, J. Suwanprateep, T. Hayakawa, K. Pugdee, Cellular responses of histatin-derived peptides immobilized titanium surface using a tresyl chloride-activated method, Dent. Mater. J. 40 (4) (2021) 934–941, https://doi.org/10.4012/dmj.2020-307.

[22] X.W. Tan, et al., Effectiveness of antimicrobial peptide immobilization for preventing perioperative cornea implant-associated bacterial infection, Antimicrob. Agents Chemother. 58 (9) (2014) 5229–5238, https://doi.org/10.1128/AAC.02859-14.

[23] M. Hoyos-Nogués, F. Velasco, M.P. Ginebra, J.M. Manero, F.J. Gil, C. Mas-Moruno, Regenerating bone via multifunctional coatings: the blending of cell integration and bacterial inhibition properties on the surface of biomaterials, ACS Appl. Mater. Interfaces 9 (26) (2017) 21618–21630, https://doi.org/10.1021/acsami.7b03127.

[24] M. Gabriel, K. Nazmi, E.C. Veerman, A.V.N. Amerongen, A. Zentner, Preparation of LL-37-grafted titanium surfaces with bactericidal activity, Bioconjugate Chem. 17 (2) (2006) 548–550, https://doi.org/10.1021/bc050091v.

[25] A. Andrea, N. Molchanova, H. Jenssen, Antibiofilm peptides and peptidomimetics with focus on surface immobilization, Biomolecules 8 (2) (2018), https://doi.org/10.3390/biom8020027.

[26] M. Godoy-Gallardo, et al., Antibacterial properties of hLf1-11 peptide onto titanium surfaces: a comparison study between silanization and surface initiated polymerization, Biomacromolecules 16 (2) (2015) 483–496, https://doi.org/10.1021/bm501528x.

[27] W. Lin, et al., Multi-biofunctionalization of a titanium surface with a mixture of peptides to achieve excellent antimicrobial activity and biocompatibility, J. Mater. Chem. B 3 (1) (2015) 30–33, https://doi.org/10.1039/c4tb01318b.

[28] S. Makihira, et al., Titanium immobilized with an antimicrobial peptide derived from histatin accelerates the differentiation of osteoblastic cell line, MC3T3-E1, Int. J. Mol. Sci. 11 (4) (2010) 1458–1470, https://doi.org/10.3390/ijms11041458.

[29] X.W. Tan, et al., Dual functionalization of titanium with vascular endothelial growth factor and β-defensin analog for potential application in keratoprosthesis, J. Biomed. Mater. Res. B Appl. Biomater. 100 (8) (2012) 2090–2100, https://doi.org/10.1002/jbm.b.32774.

[30] B. Mishra, G. Wang, Titanium surfaces immobilized with the major antimicrobial fragment FK-16 of human cathelicidin LL-37 are potent against multiple antibiotic-resistant bacteria, Biofouling 33 (7) (2017) 544–555, https://doi.org/10.1080/08927014.2017.1332186.

[31] M. Kazemzadeh-Narbat, et al., Drug release and bone growth studies of antimicrobial peptide-loaded calcium phosphate coating on titanium, J. Biomed. Mater. Res. Part B Appl. Biomater. 100 B (5) (2012) 1344–1352, https://doi.org/10.1002/jbm.b.32701.

[32] M. Kazemzadeh-Narbat, J. Kindrachuk, K. Duan, H. Jenssen, R.E.W. Hancock, R. Wang, Antimicrobial peptides on calcium phosphate-coated titanium for the prevention of implant-associated infections, Biomaterials 31 (36) (2010) 9519–9526, https://doi.org/10.1016/j.biomaterials.2010.08.035.

[33] M. Yoshinari, T. Kato, K. Matsuzaka, T. Hayakawa, K. Shiba, Prevention of biofilm formation on titanium surfaces modified with conjugated molecules comprised of antimicrobial and titanium-binding peptides, Biofouling 26 (1) (2010) 103–110, https://doi.org/10.1080/08927010903216572.

[34] P. Saporito, B. Mojsoska, A. Løbner Olesen, H. Jenssen, " Antibacterial mechanisms of GN-2 derived peptides and peptoids against Escherichia coli ,", Biopolymers 110 (6) (2019) https://doi.org/10.1002/bip.23275.

[35] B. Mojsoska, G. Carretero, S. Larsen, R.V. Mateiu, H. Jenssen, Peptoids successfully inhibit the growth of gram negative E. coli causing substantial membrane damage, Sci. Rep. 7 (February) (2017) 1–12, https://doi.org/10.1038/srep42332.

[36] B. Mojsoska, R.N. Zuckermann, H. Jenssen, Structure-activity relationship study of novel peptoids that mimic the structure of antimicrobial peptides, Antimicrob. Agents Chemother. 59 (7) (2015) 4112–4120, https://doi.org/10.1128/AAC.00237-15.

[37] J.S. Khara, et al., Ultra-short antimicrobial peptoids show propensity for membrane activity against multi-drug resistant Mycobacterium tuberculosis, Front. Microbiol. 11 (March) (2020) 1–11, https://doi.org/10.3389/fmicb.2020.00417.

[38] S. Ferraris, A. Bobbio, M. Miola, S. Spriano, Micro- and nano-textured, hydrophilic and bioactive titanium dental implants, Surf. Coating. Technol. 276 (2015) 374–383, https://doi.org/10.1016/j.surfcoat.2015.06.042.

[39] A. Lone, A. Arnous, P.R. Hansen, B. Mojsoska, H. Jenssen, Synthesis of peptoids containing multiple nhtrp and ntrp residues: a comparative study of resin, cleavage conditions and submonomer protection, Front. Chem. 8 (April) (2020) 1–12, https://doi.org/10.3389/fchem.2020.00370.

[40] Y. Iwaya, et al., Surface properties and biocompatibility of acid-etched titanium, Dent. Mater. J. 27 (3) (2008) 415–421, https://doi.org/10.4012/dmj.27.415.

[41] A. Cochis, et al., Competitive surface colonization of antibacterial and bioactive materials doped with strontium and/or silver ions, Nanomaterials 10 (1) (2020) 1–19, https://doi.org/10.3390/nano10010120.

[42] J.J. Harrison, C.A. Stremick, R.J. Turner, N.D. Allan, M.E. Olson, H. Ceri, Microtiter susceptibility testing of microbes growing on peg lids : a miniaturized biofilm model for high-throughput screening, Nat. Protoc. (2010), https://doi.org/10.1038/nprot.2010.71.

[43] S. Ferraris, et al., Surface modification of Ti-6Al-4V alloy for biomineralization and specific biological response: Part I, inorganic modification, J. Mater. Sci. Mater. Med. 22 (3) (2011) 533–545, https://doi.org/10.1007/s10856-011-4246-2.

[44] P. Mohite, et al., Chitosan and Chito-Oligosaccharide : a Versatile Biopolymer with Endless Grafting Possibilities for Multifarious Applications, 2023, pp. 1–24, https://doi.org/10.3389/fbioe.2023.1190879. May.

[45] C. Zvacek, F. Hagen, An Assessment of Catalytic Residue 3D- Ensembles for the Prediction of Enzyme Function, Master's thesis, Clemens Žváček, FernUniversität in Hagen, 2016.

[46] J. Barberi, et al., Albumin and fibronectin adsorption on treated titanium surfaces for osseointegration: an advanced investigation, Appl. Surf. Sci. 599 (June) (2022) 154023, https://doi.org/10.1016/j.apsusc.2022.154023.

[47] Y. Wang, Z. Yu, K. Li, J. Hu, Effects of surface properties of titanium alloys modified by grinding, sandblasting and acidizing and nanosecond laser on cell proliferation and cytoskeleton, Appl. Surf. Sci. 501 (October 2019) (2020) 144279, https://doi.org/10.1016/j.apsusc.2019.144279.

[48] J.O. Hollinger, AN INTRODUCTION, 2022.

[49] J.H. Cho, J.P. Garino, S.K. Choo, K.Y. Han, J.H. Kim, H.K. Oh, Seven-year results of a tapered, titanium, hydroxyapatite-coated cementless femoral stem in primary total hip arthroplasty, Clin. Orthop. Surg. 2 (4) (2010) 214–220, https://doi.org/10.4055/cios.2010.2.4.214.

[50] M.I. Froimson, J. Garino, A. Machenaud, J.P. Vidalain, Minimum 10-year results of a tapered, titanium, hydroxyapatite-coated hip stem. An independent review, J. Arthroplasty 22 (1) (2007) 1–7, https://doi.org/10.1016/j.arth.2006.03.003.

[51] L.D. Morton, D.A. Castilla-Casadiego, A.C. Palmer, A.M. Rosales, Crosslinker structure modulates bulk mechanical properties and dictates hMSC behavior on hyaluronic acid hydrogels, Acta Biomater. 155 (2023) 258–270, https://doi.org/10.1016/j.actbio.2022.11.027.

[52] A.R. Statz, J. Kuang, C. Ren, A.E. Barron, I. Szleifer, P.B. Messersmith, Experimental and theoretical investigation of chain length and surface coverage on fouling of surface grafted polypeptides, Biointerphases 4 (2) (2009) FA22–FA32, https://doi.org/10.1116/1.3115103.

[53] W. Zhao, et al., Peptoid-loaded microgels self-defensively inhibit staphylococcal colonization of titanium in a model of operating-room contamination, Adv. Mater. Interfaces 9 (31) (2022) 1–9, https://doi.org/10.1002/admi.202201662.

[54] X. Chen, J. Zhou, Y. Qian, L.Z. Zhao, Antibacterial coatings on orthopedic implants, Mater. Today Bio 19 (December 2022) (2023) 100586, https://doi.org/10.1016/j.mtbio.2023.100586.

[55] I. Masip, E. Perez-Paya, A. Messeguer, Peptoids as source of compounds eliciting antibacterial activity, Comb. Chem. High Throughput Screen. 8 (3) (2005) 235–239, https://doi.org/10.2174/1386207053764567.

[56] T. Godballe, L.L. Nilsson, P.D. Petersen, H. Jenssen, Antimicrobial β-peptides and α-peptoids, Chem. Biol. Drug Des. 77 (2) (2011) 107–116, https://doi.org/10.1111/j.1747-0285.2010.01067.x.

[57] S. Ferraris, et al., Cytocompatible and anti-bacterial adhesion nanotextured titanium oxide layer on titanium surfaces for dental and orthopedic implants, Front. Bioeng. Biotechnol. 7 (May) (2019) 1–12, https://doi.org/10.3389/fbioe.2019.00103.

[58] S. Ferraris, A. Venturello, M. Miola, A. Cochis, L. Rimondini, S. Spriano, Antibacterial and bioactive nanostructured titanium surfaces for bone integration, Appl. Surf. Sci. 311 (2014) 279–291, https://doi.org/10.1016/j.apsusc.2014.05.056.

[59] J. Lee, et al., Effect of side chain hydrophobicity and cationic charge on antimicrobial activity and cytotoxicity of helical peptoids, Bioorganic Med. Chem. Lett. 28 (2) (2018) 170–173, https://doi.org/10.1016/j.bmcl.2017.11.034.

[60] M. Lallukka, et al., Surface functionalization of Ti6Al4V-eli alloy with antimicrobial peptide nisin, Nanomaterials 12 (23) (2022), https://doi.org/10.3390/nano12234332.

[61] V. Alessandra Gobbo, et al., Functionalization of a chemically treated Ti6Al4V-ELI alloy with nisin for antibacterial purposes, Appl. Surf. Sci. 620 (November 2022) (2023) 156820, https://doi.org/10.1016/j.apsusc.2023.156820.

[62] L.R. Rivera, et al., Antibacterial, pro-angiogenic and pro-osteointegrative zein-bioactive glass/copper based coatings for implantable stainless steel aimed at bone healing, Bioact. Mater. 6 (5) (2021) 1479–1490, https://doi.org/10.1016/j.bioactmat.2020.11.001.

[63] A.G. Gristina, P.T. Naylor, Q.N. Myrvik, Biomaterial-centered infections: microbial adhesion versus tissue integration, Pathog. Wound Biomater. Infect. 7 (1981) (1990) 193–216, https://doi.org/10.1007/978-1-4471-3454-1_25.